mathematics

MDPI

Article

An Optimal Investigation of Convective Fluid Flow Suspended by Carbon Nanotubes and Thermal Radiation Impact

Dongmin Yu [1,2,3,†] and Rijun Wang [1,*]

[1] Key Laboratory of Modern Power System Simulation and Control & Renewable Energy Technology, Ministry of Education, Northeast Electric Power University, Jilin 132000, China; d.yu@neepu.edu.cn
[2] School of Information Engineering, Nanchang University, Nanchang 330027, China
[3] Beijing Key Laboratory of Demand Side Multi-Energy Carriers Optimization and Interaction Technique, China Electric Power Research Institute, Beijing 100085, China
* Correspondence: rijunwang20220311@163.com
† Northeast Electric Power University and Nanchang University are in no particular order, and they are the co-first affiliation of this paper.

Abstract: This study is focused towards analyzing the heat and flow movement among two stretching rotating disks inside water-based carbon nanotubes. The idea of thermal boundary conditions and heat convection is used and the system is expressed in partial differential equations. Using the similarity techniques, the model is successfully converted to a nonlinear ordinary differential equation. A familiar collocation method is used to simulate the outcomes of the governed system while the method is validated through a set of tables and assessed with existing literature. The physical aspects of the proposed model have been studied in detail and assisted via graphical diagrams against the variation of different parameters. It is found that the multiple-wall carbon nanotubes intensify the system quickly and improve the rate of heat transmission. It is also noted that the proposed method is in excellent in agreement with already published studies and can be extended for other physical problems. Moreover, when values of Re parameter increase, a drop is noted in the magnitude of radial velocity near the faces of the disks. It is very clear from the tabular comparison that collocation scheme is in good agreement with already published studies and homotopic solutions.

Keywords: carbon nanotubes; convective fluid flow; collocation approach; numerical solution

MSC: 34A45; 65M50; 65J15

Citation: Yu, D.; Wang, R. An Optimal Investigation of Convective Fluid Flow Suspended by Carbon Nanotubes and Thermal Radiation Impact. *Mathematics* **2022**, *10*, 1542. https://doi.org/10.3390/math10091542

Academic Editor: Antonio Lamura

Received: 11 March 2022
Accepted: 27 April 2022
Published: 4 May 2022

1. Introduction

The area of nanofluids and their extensive real-life application gained a realistic devotion among science and engineering scholars. The area of nanofluids was initiated by Choi and Eastman by introducing a new sort of thermo-fluid tag for "nanofluids" in which solid-liquid combination takes base fluid (mostly bad conductors) and solid nanometer dimensions particles—"nanoparticles" [1]. If we look at the engineering and industrial aspects then operation of nanoparticle arises in various arena, such as biological, chemotherapy, medicine, therapy, surgery, environmental, chemical, material, physical and other interdisciplinary sciences. Later on, various nanofluid models were proposed by different scholars, including Buongiorno, Xuan and Li, Tiwari and Das and Xue and Xu [2–5]. Numerous investigations have been shown with the similar ideology of studying nanofluids using different nanoparticles including aluminum oxide, copper, copper-oxide, molybdenum disulfide, silver, carbon and other shapes of carbon, such as *CNTs* [6–9]. Literature discloses that *CNTs* display outstanding motorized, ocular, electrical and thermal physiognomies [10]. *CNTs* are testified and noted as having great elasticity (500 by steel), higher current capacity (1K times) and huge density (1/2 by aluminum), compared with copper (Cu) and ample advanced conductivity (15 times). Moreover, the presence of

carbon chain *CNTs* are not risky factors and it could be useful to the scientific community and environment.

Many studies are available in the literature that deal with thermal analysis using carbon nanotubes. Hayat et al. analyzed the mixed convection flow of blood containing carbon nanotubes (*CNTs*; both single and multi-wall) over a curved stretching sheet [11]. The nanofluids-based modeling is performed through the concept of Xu idea, while dissipation and Joule heating impacts are incorporated into energy expression. Haq et al. presented viscosity and thermal conductivity of carbon nanotubes (*CNTs*) including single and multi-walls inside the base fluid of comparable volume over a fluid stream on shallow stretching [12]. Conclusions have been established in support of the entire examination and it is was discovered that engine oil-based *CNTs* have advanced skin friction and heat transmission rate compared to ethylene glycol and water-based *CNTs*. Mohyud-Din et al. analyzed the impacts of thermal radiation and carbon nanotubes (*CNTs*), both single-wall and multi-wall, in the Marangoni convection boundary-layer viscous liquid flow [13]. A numerical study using least squares methods and comparative analysis with existing method is made. Raza et al. presented an arithmetical study to pursue the influences of chemical reaction and radiation features in MHD flow of nanofluids induced by outwardly elastic diskette taking the effects of non-uniform heat sink and source [14]. The modeled equations have been efficiently solved through MATLAB-based numerical command and outcomes analysis is reported via graphical plots. Haq et al. explored a study to seek the impacts of volume fraction of carbon nanotubes (*CNTs*) on magneto-hydrodynamics stream and heat transmission in dual cross directions over a stretching sheet with convective boundary conditions [15]. Three sorts of base fluids including water, ethylene glycol and engine oil are used and compared while impacts of single and multi-wall carbon nanotubes were studied. The readers can obtain more information on the topic in [16–24].

Hamid et al. explored the hydromagnetic flow and heat control inside a partly heated rectangular fin-shaped cavity containing carbon nanotubes (*CNTs*) incorporated in water [25]. A tiny intense (heated) rod is located in the interior of the cavity to generate a heat transfer source or a resistance. The right wall of the horizontal tip is tested for three dissimilar temperatures (adiabatic, cold and heated). Experimental validation of the study was made and results are explained physically using graphs. It is found that the velocity components are maximum and minimum at the vertical and horizontal corners, respectively. The local Nusselt numbers are improved by incorporating both radiations impacts and solid volume fraction of *CNTs*, whereas, peak of the Nusselt number is noted at the corners. Khan et al. examined the properties of water-based single-walled carbon nanotubes on free-convection in a partially heated right trapezoidal cavity where the lower boundary is heated while the side and top walls are kept cold and adiabatic, respectively [26]. The proposed dimensionless partial differential equations are explained with designated dimensionless boundary conditions via a finite element scheme and outcomes are illustrated graphically. The readers can see the references to understand the study of nanofluids inside the complex enclosures [27–37].

The motivation of current research work is to examine the heat and flow movement among two stretching rotating disks inside the water-based carbon nanotubes. The idea of thermal boundary conditions and heat convection is used and the system is expressed in partial differential equations. The considered model has significance in real life, such as the governing model used in ground water flows, geothermal extraction, storage of nuclear waste material, oil recovery processes, impurity dispersion in aquifers, etc. A comprehensive assessment of outcomes gained by collocation and RK-4 methods is made to display the competence of recommended procedures. The physical aspects of the proposed model were studied in detail and asserted via graphical diagrams by variation in different parameters. It is found that the multiple-wall carbon nanotubes intensify the system quickly and improve the rate of heat transmission. It is also noted that the proposed method is in excellent agreement with already published studies and homotopic solutions and can be extended for other physical problems [38].

2. Mathematical Formulation

Assuming the flow of nanofluid among double nonequivalent immeasurable disks that are axisymmetric and incompressible, both plates disconnected by h (constant distance), one is at a point $z = 0$ and $z = h$ is the location of the other. Assuming the disks are revolving with the angular velocities towards the axial direction, for the first one it is Ω_1 and the velocity of second is Ω_2. Figure 1 is shown to understand the geometrical aspect of the problem. It can be seen that stretching rates of the disks are, respectively, a_1 and a_2 in the radial direction. Two sorts of carbon nanotubes (single and multi-wall) were employed as nanoparticles inside water-based fluid. In addition, the surface validates the convective type boundary conditions. Moreover, it is further assumed that that temperature of the upper and lower disks is T_1 and T_0. Taking all assumptions into consideration, the governing equations of the mechanism in cylindrical coordinates are [20]:

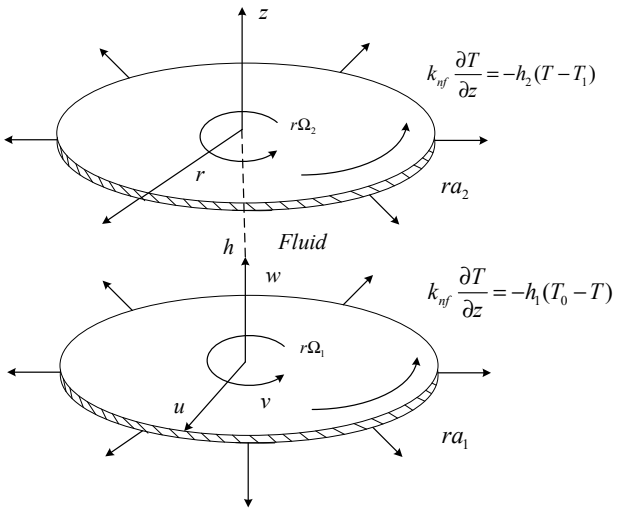

Figure 1. Systematic diagram of the problem [39,40].

$$\frac{\partial u}{\partial r} + \frac{\partial w}{\partial z} + \frac{u}{r} = 0, \tag{1}$$

$$u\frac{\partial u}{\partial r} - \frac{v^2}{r} + w\frac{\partial u}{\partial z} = -\frac{1}{\rho_{nf}}\left(\frac{\partial p}{\partial r}\right) + \nu_{nf}\left(\frac{\partial^2 u}{\partial r^2} + \frac{\partial^2 u}{\partial z^2} + \frac{1}{r}\frac{\partial u}{\partial r} - \frac{u}{r^2}\right), \tag{2}$$

$$u\frac{\partial v}{\partial r} + \frac{uv}{r} + w\frac{\partial v}{\partial z} = \nu_{nf}\left(\frac{\partial^2 v}{\partial r^2} + \frac{\partial^2 v}{\partial z^2} + \frac{1}{r}\frac{\partial v}{\partial r} - \frac{v}{r^2}\right), \tag{3}$$

$$w\frac{\partial w}{\partial z} + u\frac{\partial w}{\partial r} = \nu_{nf}\left(\frac{\partial^2 w}{\partial r^2} + \frac{\partial^2 w}{\partial z^2} + \frac{1}{r}\frac{\partial w}{\partial r}\right) - \frac{1}{\rho_{nf}}\frac{\partial p}{\partial z}, \tag{4}$$

$$\left(\rho c_p\right)_{nf}\left[w\frac{\partial T}{\partial z} + u\frac{\partial T}{\partial r}\right] = k_{nf}\left(\frac{1}{r}\frac{\partial T}{\partial r} + \frac{\partial^2 T}{\partial r^2} + \frac{\partial^2 T}{\partial z^2}\right) + \frac{16\sigma^* T_1^3}{3k^*}\left(\frac{1}{r}\frac{\partial T}{\partial r} + \frac{\partial^2 T}{\partial r^2} + \frac{\partial^2 T}{\partial z^2}\right), \tag{5}$$

associated with the following boundary conditions

$$z \to 0 \; then \; v = r_1\Omega_1, k_{nf}\frac{\partial T}{\partial z} = (T_0 - T)(-h_1), u = r_1 a_1 \; w = 0, \tag{6}$$

$$z \to h \; then \; v = r_1\Omega_2, u = r_1 a_2, \; k_{nf}\frac{\partial T}{\partial z} = (T - T_1)(-h_2), \; w = 0, \tag{7}$$

where some parameters are indicated, such as mean absorption coefficient (k^*), fluid temperature (T), pressure (p) and Stefan Boltzmann constant (r_1). The h_2 and h_1 are, respectively, represented as convective heat transfer coefficients of upper and at lower walls.

$$\mu_{nf} = \frac{\mu_f}{(1-\phi)^{2.5}}, \rho_{nf} = \rho_{CNT}(\phi) + \rho_f(1-\phi), \left(\rho c_p\right)_{nf} = \left(\rho c_p\right)_{CNT}(\phi) + \left(\rho c_p\right)_f(1-\phi), \frac{k_{nf}}{k_f} = \frac{(-\phi+1)+2\phi ln ln\ \frac{k_{CNT}+k_f}{2k_f}\ \frac{k_{CNT}}{k_{CNT}-k_f}}{(-\phi+1)+2\phi ln ln\ \frac{k_{CNT}+k_f}{2k_f}\ \frac{k_f}{k_{CNT}-k_f}}. \tag{8}$$

In the equation above the parameters $\rho,\ \mu, k$ and c_p are density, nanofluid effective dynamic viscosity, thermal conductivity and heat capacitance. Moreover, the solid volume fraction of nanoparticles, thermo-based physical possessions of base fluid, nanofluid and carbon nanotubes are correspondingly designated as $\phi,\ f, nf$ and CNT. To change the directly-above structure of the partial differential equations (PDEs) to a nonlinear ordinary differential equations set we have considered the subsequent alteration schemes:

$$v = r\Omega_1 g(\eta),\ u = r\Omega_1 f'(\eta),\ w = -2h\Omega_1 f(\eta), \quad \frac{T-T_1}{T_0-T_1} = \theta(\eta),\ \frac{z}{h} = \eta,\ \rho_f \Omega_1 \nu_f \left(\frac{1}{2}\frac{r^2}{h^2}\epsilon + P(\eta)\right) = p. \tag{9}$$

Assisted by the similarity viable equations in (9), we have gained (1)–(7):

$$\frac{1}{(1-\phi)^{2.5}\left(1-\phi+\frac{\rho_{CNT}}{\rho_f}\phi\right)} f''' + Re\left(2ff'' - f'^2 + g^2\right) - \frac{\epsilon}{1-\phi+\frac{\rho_s}{\rho_f}\phi} = 0, \tag{10}$$

$$\frac{1}{(1-\phi)^{2.5}\left(1-\phi+\frac{\rho_{CNT}}{\rho_f}\phi\right)} g'' + 2Re\left(fg' - f'g\right) = 0, \tag{11}$$

$$\frac{1}{\left(1-\phi+\frac{\rho_{CNT}}{\rho_f}\phi\right)} P' = -4Reff' - \frac{2}{(1-\phi)^{2.5}\left(1-\phi+\frac{\rho_{CNT}}{\rho_f}\phi\right)} f'' = 0, \tag{12}$$

$$\frac{1}{Pr}\left(\frac{k_{nf}}{k_f} + Rd\right)\theta'' + 2Re\left(1-\phi+\frac{\left(\rho c_p\right)_{CNT}}{\left(\rho c_p\right)_f}\phi\right) f\theta' = 0. \tag{13}$$

The boundary conditions obtained as:

$$f(\eta) = 0,\ P(\eta) = 0, g(\eta) = 1,\ f'(\eta) = A_1, \theta'(\eta) = -\frac{k_f}{k_{nf}}\gamma_1[1-\theta(\eta)], \eta \to 0, \quad \theta'(\eta) = -\frac{k_f}{k_{nf}}\gamma_2\theta(\eta),\ f'(\eta) = A_2, f(\eta) = 0,\ g(\eta) = \Omega, \eta \to 0, \tag{14}$$

In the above-described reduced system, involved parameters are, Reynold number (Re), Prandtl number (Pr), scaled stretching ($A_1 and\ A_2$), Biot (Bi), rotation parameter (Ω) and radiation parameter (Rd).

$$\frac{\left(\rho c_p\right)_f \nu_f}{k_f} = Pr, \frac{\Omega_1 h^2}{\nu_f} = Re,\ \frac{a_1}{\Omega_1} = A_1, \frac{a_2}{\Omega_1} = A_2, \frac{16\sigma^* T_1^3}{3k_f k^*} = Rd, \frac{\Omega_2}{\Omega_1} = \Omega,\ \frac{hh_1}{k_f} = \gamma_1,\ \frac{hh_2}{k_f} = \gamma_2.$$

Now taking the derivative of the expression, (10) with respect to η and then eliminating ϵ, we found the simple model as follows:

$$\frac{1}{(1-\phi)^{2.5}\left(1-\phi+\frac{\rho_{CNT}}{\rho_f}\phi\right)} f^{iv} + 2Re\left(ff''' + gg'\right) = 0, \tag{15}$$

and ϵ can be obtained by considering the subsequent expression as

$$\epsilon = \frac{1}{(1-\phi)^{2.5}} f'''(0) - Re\left(1-\phi+\frac{\rho_{CNT}}{\rho_f}\phi\right)\left[\left(f'(0)\right)^2 - (g(0)) + \frac{M}{\left(1-\phi+\frac{\rho_{CNT}}{\rho_f}\phi\right)}\frac{\sigma_{nf}}{\sigma} f'(0)\right],$$

Now, integration of Equation (12) will give us the solution for the involved pressure as given below:

$$-2\left[Re\left(f^2\right)+\left(f'-f'(0)\right)\frac{1}{(1-\phi)^{2.5}\left(1-\phi+\frac{\rho_{CNT}}{\rho_f}\phi\right)}\right]=\frac{1}{\left(1-\phi+\frac{\rho_{CNT}}{\rho_f}\phi\right)}P.$$

The entire shear-stress at the bottom disk can be calculated using the expression:

$$\tau_w=\sqrt{\tau_{zr}^2+\tau_{z\theta}^2},$$

where τ_{zr} and $\tau_{z\theta}$ indicate the radial and tangential directions of shear stress and are defined as:

$$\tau_{zr}=\mu_{nf}\,\frac{\partial u}{\partial z}|_{z=0}=\frac{\mu_f r\Omega_1 f''(0)}{(1-\phi)^{2.5}h},\ \tau_{z\theta}=\mu_{nf}\,\frac{\partial v}{\partial z}|_{z=0}=\frac{\mu_f r\Omega_1 g'(0)}{(1-\phi)^{2.5}h}.$$

At lower and upper disks the skin friction coefficients C_1 and C_2 are given as:

$$\frac{1}{Re_r(1-\phi)^{2.5}}\left[\left(g'(0)\right)^2+\left(f''(0)\right)^2\right]^{\frac{1}{2}}=\frac{\tau_w|_{z=0}}{\rho_f(r\Omega_1)^2}=C_1,$$

$$\frac{1}{Re_r(1-\phi)^{2.5}}\left[\left(g'(1)\right)^2+\left(f''(1)\right)^2\right]^{\frac{1}{2}}=\frac{\tau_w|_{z=h}}{\rho_f(r\Omega_2)^2}=C_2.$$

Local Reynolds numbers are calculated as $\frac{r\Omega_1 h}{\nu_f}=Re_r$. The upper disk and lower disk have heat transmission as follows:

$$\frac{hq_r}{k_f(T_0-T_1)}|_{z=h}=Nu_{x2},\ \frac{hq_w}{k_f(T_0-T_1)}|_{z=0}=Nu_{x1}$$

Here q_r and q_w are the radiative and wall heat flux specified under:

$$q_w|_{z=h}=q_r|_{z=h}-k_{nf}\frac{\partial T}{\partial z}|_{z=h},q_w|_{z=0}=q_r|_{z=0}-k_{nf}\frac{\partial T}{\partial z}|_{z=0},$$

$$\frac{16\sigma^* T_1^3}{3k^*}\frac{\partial T}{\partial z}|_{z=0},=q_r|_{z=0},\ \frac{16\sigma^* T_1^3}{3k^*}\frac{\partial T}{\partial z}|_{z=h}=q_r|_{z=h}.$$

The Nusselt numbers at lower and upper disks in dimensionless form are given as:

$$Nu_2=-\theta'(1)\left(\frac{k_{nf}}{k_f}+Rd\right),-\left(Rd+\frac{k_{nf}}{k_f}\right)\theta'(0)=Nu_1.$$

3. Methodology and Solution Procedure

Numerical analysis of the considered convective fluid flow suspended by the carbon nanotubes by means of the well-known and efficient collocation approach; this scheme is very simple to apply and has the following procedure for the obtained set of dimensionless equations:

Step 1. Let start with considering the following dimensionless form

$$f^{iv}(\eta)+2Re(1-\phi)^{2.5}\left(1-\phi+\frac{\rho_{CNT}}{\rho_f}\phi\right)\left(f(\eta)f'''(\eta)+g(\eta)g'(\eta)\right)=0, \tag{16}$$

$$g''(\eta)+2Re(1-\phi)^{2.5}\left(1-\phi+\frac{\rho_{CNT}}{\rho_f}\phi\right)\left(f(\eta)g'(\eta)-f'(\eta)g(\eta)\right)=0, \tag{17}$$

$$\frac{1}{Pr}\left(\frac{k_{nf}}{k_f}+Rd\right)\theta''(\eta)+2Re\left(1-\phi+\frac{(\rho c_p)_{CNT}}{(\rho c_p)_f}\phi\right)f(\eta)\theta'(\eta)=0. \tag{18}$$

Step 2. This scheme allows us to write the following approximate solutions to find the solutions of the problems defined in step 1 as below:

$$\widetilde{f}=a_0+a_1\eta+a_2\eta^2+\ldots+a_M\eta^M=\sum_{k=0}^{M}a_k\eta^k, \tag{19}$$

$$\widetilde{g}=b_1+b_2\eta+b_3\eta^2+\ldots+b_M\eta^M=\sum_{k=0}^{M}b_k\eta^k, \tag{20}$$

$$\widetilde{\theta}=c_1+c_2\eta+c_3\eta^2+\ldots+c_M\eta^M=\sum_{k=0}^{M}c_k\eta^k. \tag{21}$$

Here the parameter M denotes the order of approximation via collocation method, and it is well known that as we enhance the value of M, the accuracy improves gradually. After imposing the obtained dimensionless boundary conditions on the above trial solution, it converts to the following modified form and we call it modified trial solutions:

$$\widetilde{f}=A_1\eta-(A_2+2A_1)\eta^2+(A_2+A_1)\eta^3+\sum_{k=1}^{M}a_k\Big(k-(k+1)\eta+\eta^{k+1}\Big)\eta^2, \tag{22}$$

$$\widetilde{g}=1-(1-\Omega)\eta-\sum_{k=1}^{M}b_k\Big(1-\eta^k\Big)\eta, \tag{23}$$

$$\begin{aligned}\widetilde{\theta}&=\tfrac{\gamma_1}{R}\Big(k_{nf}+\gamma_2k_f\Big)-\tfrac{k_f\gamma_2\gamma_1}{R}\eta\\&+\sum_{k=1}^{M}c_k\Big(\eta^{k+1}-\tfrac{1}{R}\Big(\gamma_1\eta+\tfrac{k_{nf}}{k_f}\Big)\Big((k+1)k_{nf}+\gamma_2k_f\Big)\Big).\end{aligned} \tag{24}$$

where $R=(\gamma_1+\gamma_2)k_{nf}+\gamma_1\gamma_2k_f$.

Step 3. We can generate the residual functions R_f, R_g and R_θ by incorporating the modified trial solutions into the problem give in step 1, obtaining the following form as:

$$R_f=f^{iv}(\eta)+2Re(1-\phi)^{2.5}\left(1-\phi+\frac{\rho_{CNT}}{\rho_f}\phi\right)\big(f(\eta)f'''(\eta)+g(\eta)g'(\eta)\big)\neq 0, \tag{25}$$

$$R_g=g''(\eta)+2Re(1-\phi)^{2.5}\left(1-\phi+\frac{\rho_{CNT}}{\rho_f}\phi\right)\big(f(\eta)g'(\eta)-f'(\eta)g(\eta)\big)\neq 0, \tag{26}$$

$$R_\theta=\frac{1}{Pr}\left(\frac{k_{nf}}{k_f}+Rd\right)\theta''(\eta)+2Re\left(1-\phi+\frac{(\rho c_p)_{CNT}}{(\rho c_p)_f}\phi\right)f(\eta)\theta'(\eta)\neq 0. \tag{27}$$

Step 4. In order to investigate the unknowns present in the set of residual functions given above, it is necessary to generate the set of algebraic equations which are equal in the number the unknowns present in R_f, R_g and R_θ, therefore we use the following equal spaced collocation points:

$$\eta_l=a+\frac{1}{M}l,\ l=0,1,2,3,\ldots,M.$$

Step 5. After solving the system of algebraic equations obtained in step 4, we achieved the values of unknowns, and inserting these constants into the above modified trial solution yields the numerical solution of nondimensional form of the governing model.

In order to see the impact of numerous parameters on the velocities and temperature profiles, we simulate the collocation method Maple code against $M = 7$ and $\phi = 0.2$, $Re = 0.9$, $\gamma_1 = 0.4$, $\gamma_2 = 0.5$, $A_1 = 0.7$, $Pr = 1$, $\Omega = A_2 = 0.8$.

4. Results and Discussion

The model is numerically examined using the efficient collocation method and the behavior of the profiles including velocity (tangential and axial) and temperature and is shown graphically against the variation of various prominent parameters including the dimensionless form [41–45]. The numerical simulations are made for $M = 7$ and $\phi = 0.2$, $Re = 0.9$, $\gamma_1 = 0.4$, $\gamma_2 = 0.5$, $A_1 = 0.7$, $Pr = 1$, $\Omega = A_2 = 0.8$. Figure 2 illustrates the velocities attitude against Re parameters. Figure 2a,c has been respectively asserted to show the behavior of axial $f(\eta)$ and tangential velocities $g(\eta)$ with *SWCNTs* while the axial $f(\eta)$ and tangential velocities behavior in the presence of *MWCNTs* is displayed in Figure 2b,d, respectively. The temperature profile is analyzed and plots for *SWCNTs* and *MWCNTs* are displayed in Figure 2b and Figure 3a, respectively. The impact of nanoparticles volume friction ϕ on the velocities is illustrated in Figure 4a for the axial case and Figure 4c for the tangential case in the presence of *SWCNTs* while Figure 4b,d respectively display the behavior for axial and tangential velocities with the incorporation of *MWCNTs*. Figure 5a,b is plotted to seek the temperature analysis against the nanoparticles volume friction ϕ. It can be seen that the ϕ impact with *SWCNTs* is depicted in Figure 5a, while the ϕ impact with *SWCNTs* is presented in Figure 5b. Consequences of parameter A_1 on radial velocity are offered in Figure 6a,b for *SWCNTs* and *MWCNTs*, correspondingly. We detected that the dual influence of parameter A_1 on $f'(\eta)$. The radial velocity shape surges upwards as parameter A_1 is improved while $0 \leq \eta < 3.35$, when $3.35 \leq \eta \leq 1$ the radial velocity profile drops when parameter A_1 increases. Analogous profile of $f'(\eta)$ is attained for *SWCNTs* and *MWCNTs*. Figure 7a,b is plotted to depict the effect of parameter A_2 of $f(\eta)$ for the *SWCNTs* and *MWCNTs*, separately. As parameter A_2 is boosted the axial velocity drops near the surface of the lower disk. A similar profile for $f'(\eta)$ is achieved for *SWCNTs* and *MWCNTs*. Figure 8a,b demonstrate that the tangential velocity profile is a growing function of parameter A_2 for *SWCNTs* and *MWCNTs*, correspondingly. The magnitude of $g(\eta)$ has greater values of *SWCNTs* compared to *MWCNTs*.

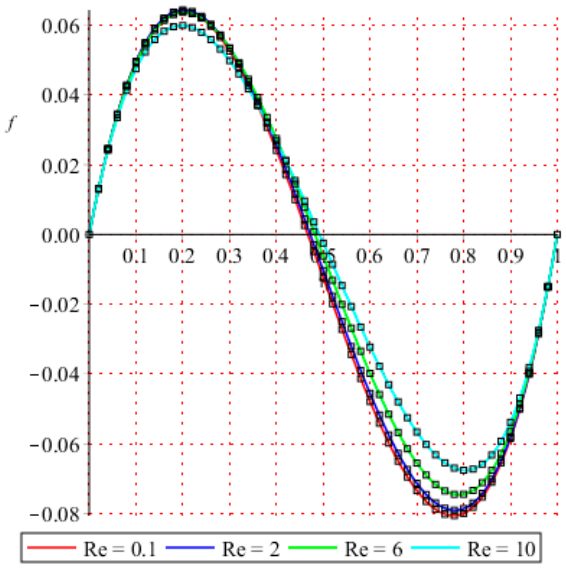

(**a**)

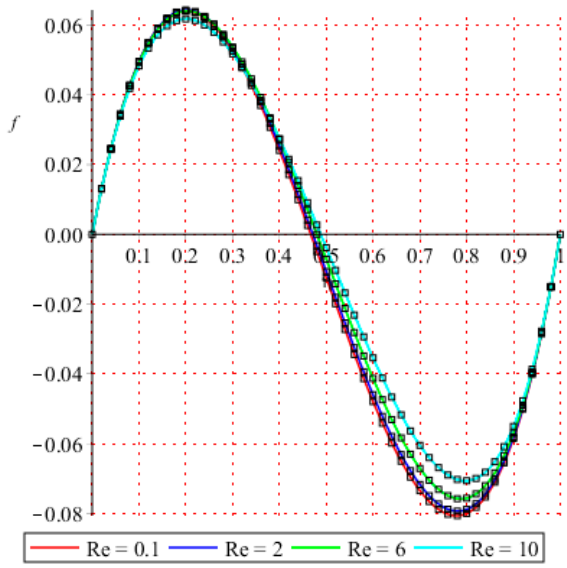

(**b**)

Figure 2. *Cont.*

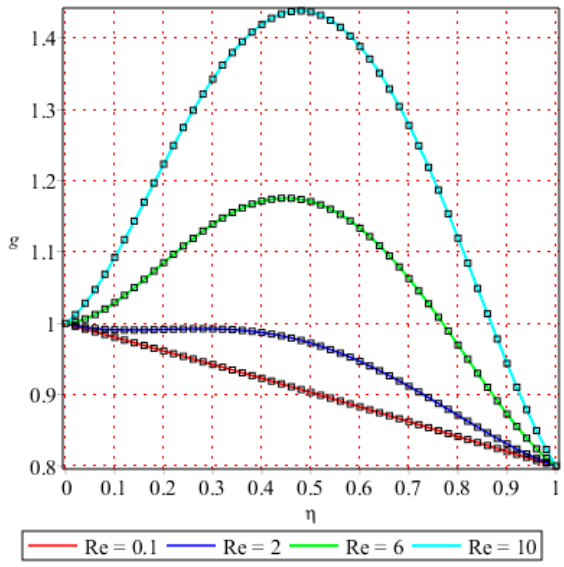

(**c**)

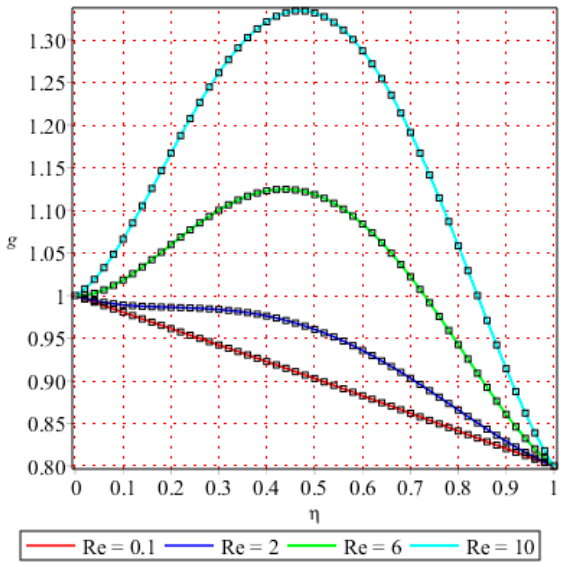

(**d**)

Figure 2. Influence of Re on velocities (**a**,**b**). Axial $f(\eta)$. (**c**,**d**). Tangential $g(\eta)$. (**a**) *SWCNTs*, (**b**) *MWCNTs*, (**c**) *SWCNTs*, (**d**) *MWCNTs*.

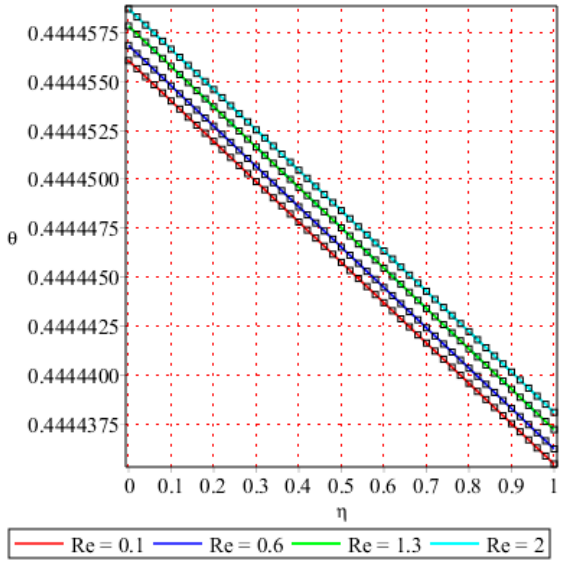

(**a**)

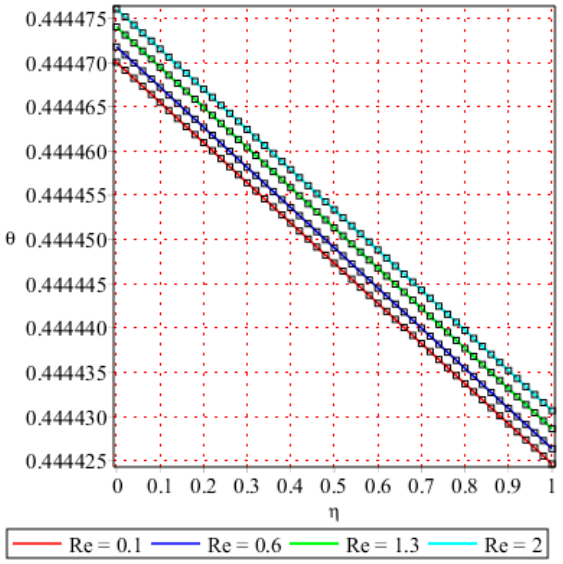

(**b**)

Figure 3. Influence of Re on (**a**,**b**). Temperature $\theta(\eta)$. (**a**) *SWCNTs*, (**b**) *MWCNTs*.

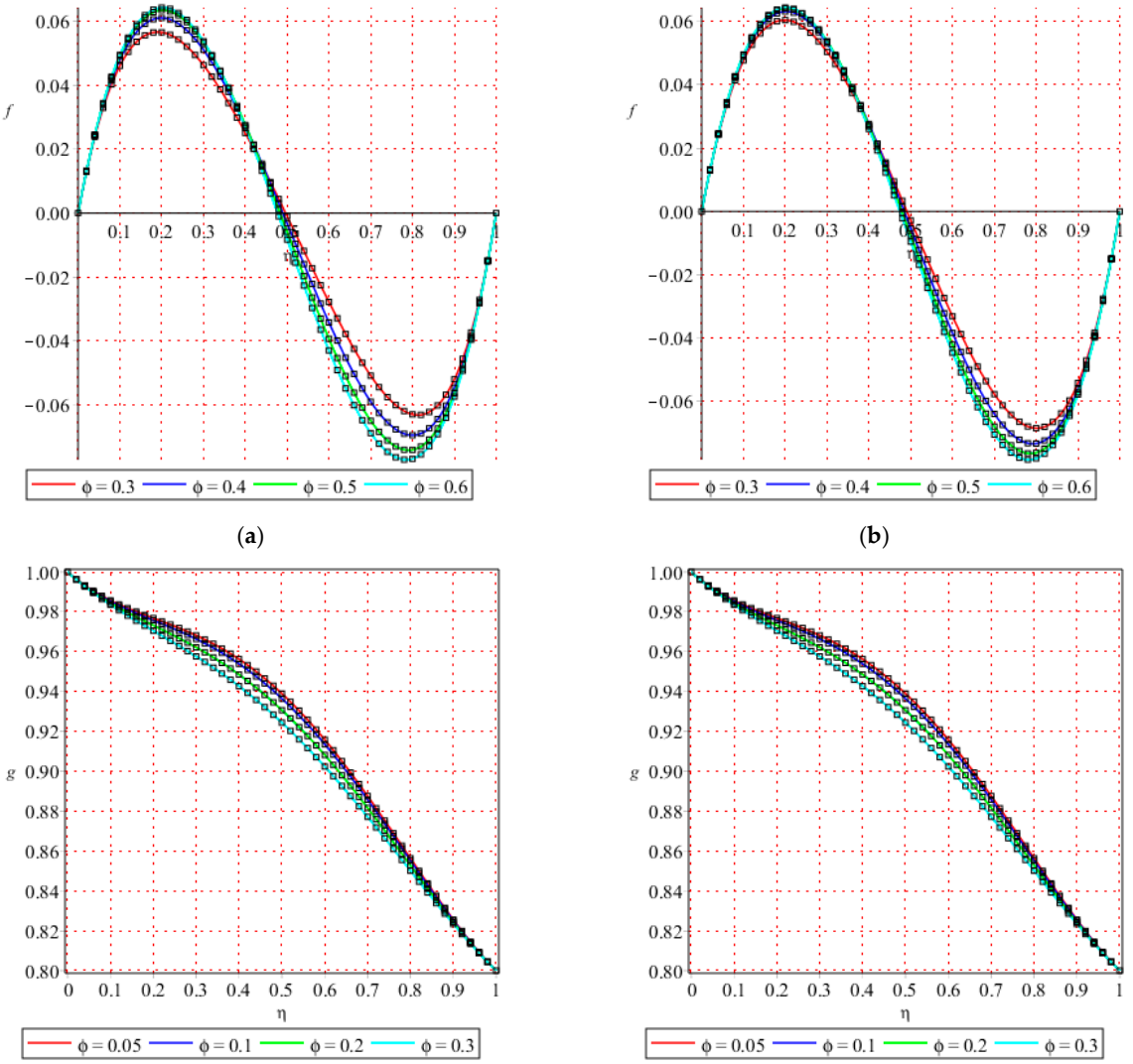

Figure 4. Influence of ϕ on velocities (**a**,**b**). Axial $f(\eta)$. (**c**,**d**) Tangential $g(\eta)$. (**a**) *SWCNTs*, (**b**) *MWCNTs*, (**c**) *SWCNTs*, (**d**) *MWCNTs*.

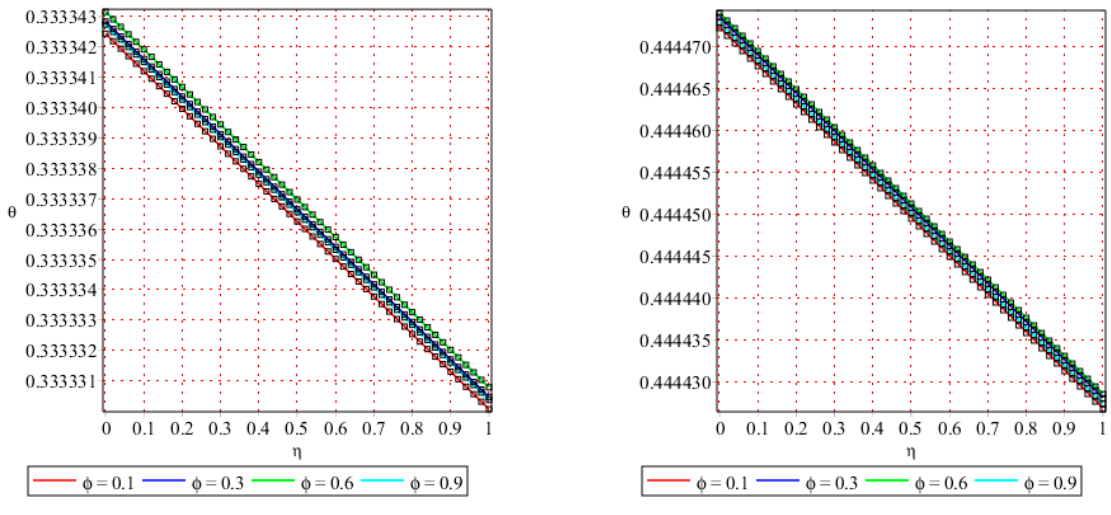

Figure 5. Influence of ϕ on temperature $\theta(\eta)$. (**a**) *SWCNTs*, (**b**) *MWCNTs*.

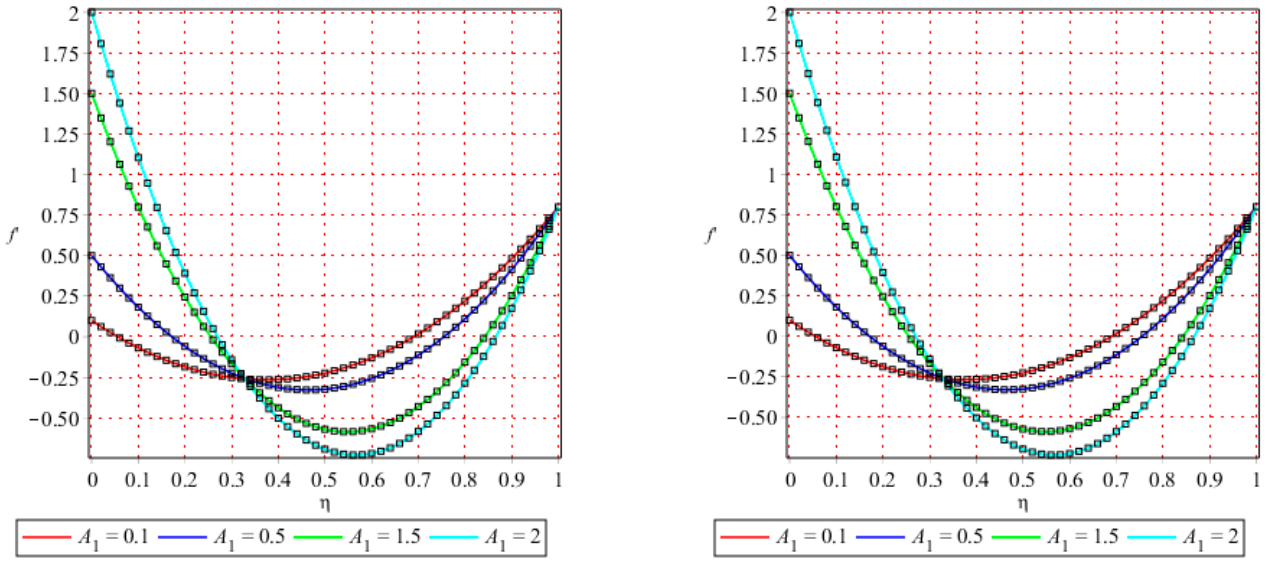

(**a**) (**b**)

Figure 6. Influence of A_1 on $f'(\eta)$. (**a**) *SWCNTs*, (**b**) *MWCNTs*.

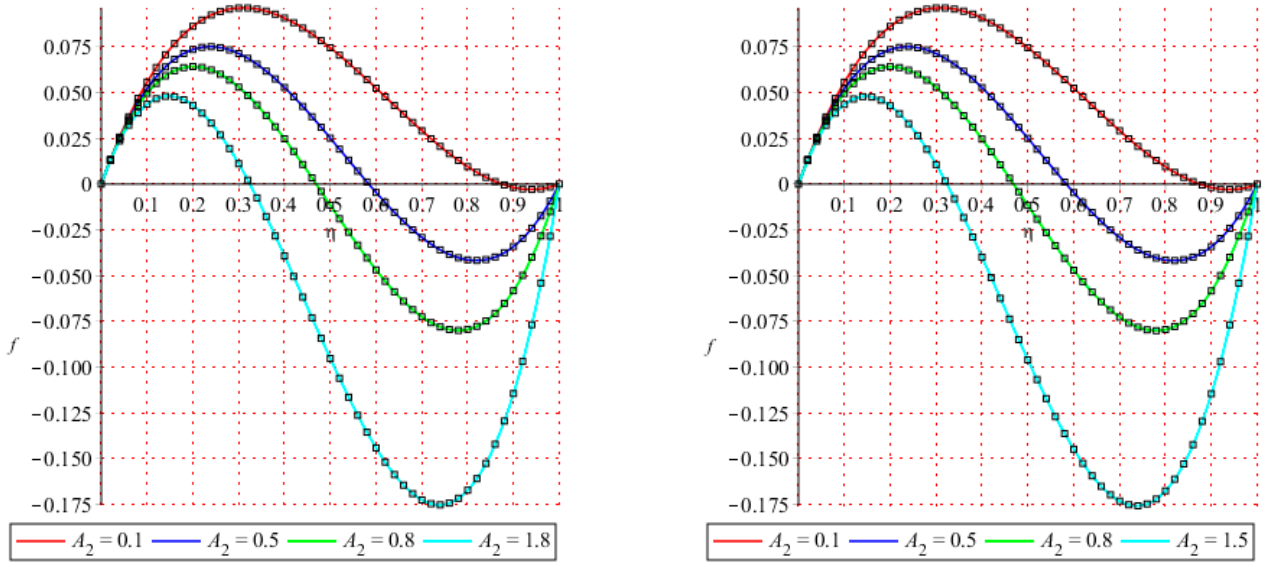

(**a**) (**b**)

Figure 7. Influence of A_2 on $f(\eta)$. (**a**) *SWCNTs*, (**b**) *MWCNTs*.

Table 1 is construct to show the thermo-physical properties. Comparative study is made for various values of involved parameters with other methods and existing physical outcomes while a detailed sketch is available in Table 2. The table is particularly made for $\phi = A_1 = A_2 = 0$, $Re = 1$ and for different values of Ω. It is very clear from the tabular comparison given in Table 2 that the collocation scheme is in good agreement with already published studies and homotopic solutions. In Table 3, by taking various values for M, when $\phi = 0.2$, $A_1 = 0.7$, $\gamma_2 = 0.5$, $\gamma_1 = 0.4$, $\Omega = A_2 = 0.8$, $Rd = 0.3$ and $Re = 0.9$. an extensive study related to error investigation for axil and tangential velocities, and temperature profile with *SWCNTs*, was made. It can be seen in Table 3 that higher values of M allow for a better analysis of the problem and accuracy level is improved at tangible level. Table 4 is given to display the convergence analysis of the proposed scheme when $\phi = 0.2$, $Re = 0.9$, $\gamma_1 = 0.4$, $\gamma_2 = 0.5$, $A_1 = 0.7$, $\Omega = A_2 = 0.8$, $Pr = 6.2$ and $Rd = 0.3$. Table 5 is constructed to show the effectiveness of the proposed method. In this

table, residual error of velocity, temperature and concentration profile is shown against the variation of M. It is important to note that as the value of M is enhanced the residual error decreases gradually, this shows the convergence of the proposed method.

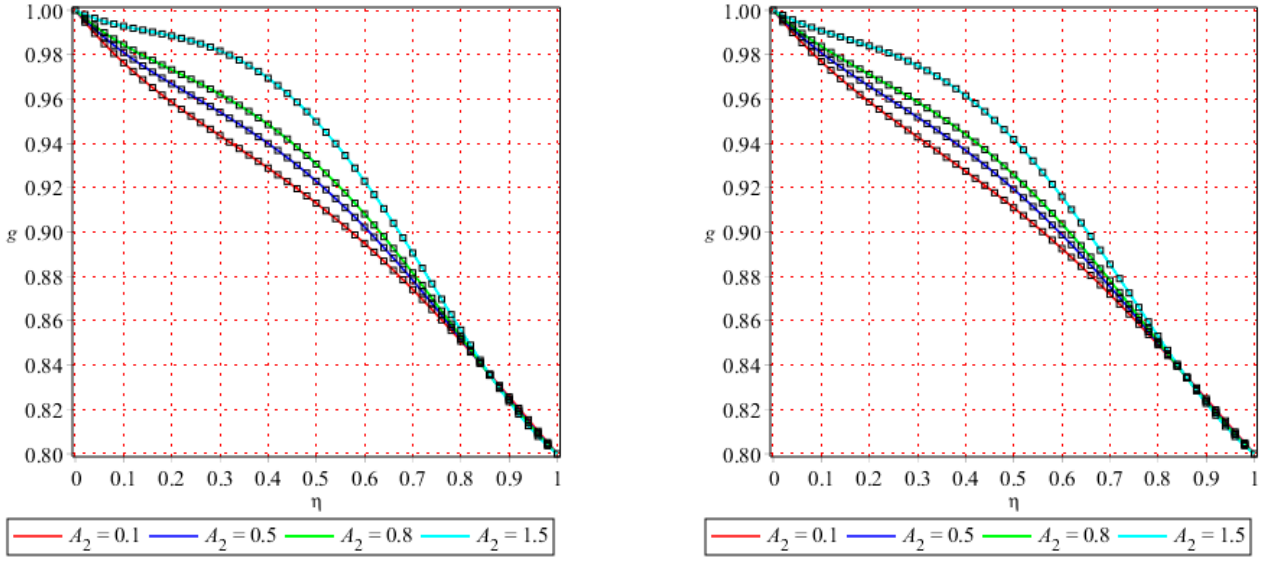

Figure 8. Influence of A_2 on $g(\eta)$. (**a**) *SWCNTs*, (**b**) *MWCNTs*.

Table 1. Thermo-physical properties of water and carbon nanotube.

Thermophysical Properties	k (W/mK)	ρ (kg/m^3)	$c_p(J/kgK)$
Water	0.613	997.1	4179
SWCNTs	6600	2600	425
MWCNTs	3000	1600	796

Table 2. Assessment of the projected outcomes for $f''(0)$ and $g'(0)$ with existing results [39] and homotopic analysis method (HAM) [40] for $\phi = A_1 = A_2 = 0$, $Re = 1$ and for different values of Ω.

Ω	[40]	[39]	CM	[40]	[39]	CM
–	0.06666	0.06666	0.06666314	2.00095	2.00095	2.00095204
−0.8	0.08394	0.08394	0.08394207	1.80259	1.80259	1.80258842
−0.3	0.10395	0.10395	0.10395088	1.30442	1.30442	1.30442358
0	0.09997	0.09997	0.09997221	1.00428	1.00428	1.00427759
0.5	0.06663	0.06663	0.06663420	0.50261	0.50261	0.50261352

Table 3. Error investigation of axil and tangential velocities, and temperature profiles for *SWCNTs* for dissimilar values of when $\phi = 0.2$, $A_1 = 0.7$ $\gamma_2 = 0.5$, $\gamma_1 = 0.4$, $\Omega = A_2 = 0.8$, $Rd = 0.3$, and $Re = 0.9$.

k	M	$Error_f$	$Error_g$	$Error_\theta$
1	08	1.71536×10^{-10}	6.93642×10^{-11}	3.84831×10^{-26}
	13	5.81908×10^{-14}	1.09435×10^{-16}	9.29935×10^{-31}
	18	4.23987×10^{-19}	4.41625×10^{-22}	1.38211×10^{-36}
	22	2.13039×10^{-24}	1.28969×10^{-27}	1.93124×10^{-42}
	26	1.26154×10^{-31}	1.66696×10^{-35}	2.17492×10^{-50}
	30	2.26778×10^{-35}	4.89294×10^{-39}	3.27934×10^{-53}

Table 4. Convergence of the proposed method when $\phi = 0.2$,$Re = 0.9$, $\gamma_1 = 0.4$, $\gamma_2 = 0.5$, $A_1 = 0.7$,$\Omega = A_2 = 0.8$,$Pr = 6.2$ and $Rd = 0.3$.

	SWCNTs			*MWCNTs*		
M	$-f''(0)$	$-g'(0)$	$-\theta'(0)$	$-f''(0)$	$-g'(0)$	$-\theta'(0)$
1	4.4213991	0.6357312	0.0000206393047	4.4130586	0.5695951	0.0000454053457
4	4.3936648	0.1928291	0.0000206392404	4.3942372	0.1945842	0.0000454050291
7	4.3937727	0.1938640	0.0000206392413	4.3943129	0.1953145	0.0000454050328
10	4.3938406	0.1938180	0.0000206392413	4.3943621	0.1952809	0.0000454050330
15	4.3938407	0.1938198	0.0000206392413	4.3943621	0.1952819	0.0000454050330
21	4.3938407	0.1938198	0.0000206392413	4.3943621	0.1952819	0.0000454050330
23	4.3938407	0.1938198	0.0000206392413	4.3943621	0.1952819	0.0000454050330
28	4.3938407	0.1938198	0.0000206392413	4.3943621	0.1952819	0.0000454050330
31	4.3938407	0.1938198	0.0000206392413	4.3943621	0.1952819	0.0000454050330

Table 5. Error analysis of axil velocity, tangential velocity and temperature for *SWCNTs* for different values of M.

k	M	ϵ_f	ϵ_g	ϵ_θ
1	10	2.10474×10^{-10}	6.10471×10^{-11}	7.36521×10^{-26}
	15	1.50471×10^{-14}	3.66540×10^{-16}	1.54891×10^{-31}
	19	5.00474×10^{-19}	4.45874×10^{-22}	1.05478×10^{-36}
	23	1.33691×10^{-24}	1.75325×10^{-27}	2.69801×10^{-42}
	28	1.00081×10^{-31}	9.35682×10^{-35}	2.45701×10^{-50}
	31	2.12453×10^{-35}	4.00147×10^{-39}	3.00689×10^{-53}

5. Concluding Remarks

This study is carried out to examine the heat and flow measure among two stretching rotating disks containing the water-based carbon nanotubes. The concept of thermal boundary conditions and heat convection is utilized and the system is expressed in partial differential equations. By means of the similarity methods, the model is fruitfully changed to a nonlinear ordinary differential equation. A familiar collocation method is used to simulate the outcomes of the governed system while the method is validated through a set of tables and assessment with existing literature.

Hence, significant observations are given below:

- When the values of Re parameter are increased, a drop is noted in the magnitude of radial velocity near the faces of the disks.
- It is very clear from the tabular comparison given in Table 2 that the collocation scheme is in good agreement with already published studies and homotopic solutions.
- It is found that the multiple-wall carbon nanotubes intensify the system quickly and improve the rate of heat transmission.
- It is also noted that the proposed method is in excellent agreement with already published studies and homotopic solutions and can be extended for other physical problems.

Author Contributions: Conceptualization, methodology, validation, formal analysis, investigation, resources, data curation, writing—original draft preparation, writing—review and editing, visualization, supervision, project administration and funding acquisition, D.Y. and R.W. All authors have read and agreed to the published version of the manuscript.

Funding: This research was funded by Nanchang University.

Institutional Review Board Statement: Not applicable.

Informed Consent Statement: Not applicable.

Data Availability Statement: Not applicable.

Conflicts of Interest: The authors declare no conflict of interest.

Nomenclature

h	Distance between the plates
Ω_1 and Ω_2	Angular velocities of the plates
a_1 and a_2	Stretching rates in radial direction
T_1 and T_0	Temperature of upper and lower disks
k^*	Mean absorption coefficient
T	Fluid temperature
p	Pressure
r_1	Stefan Boltzmann constant
h_2 and h_1	Convective heat transfer coefficients at upper and at lower walls
ρ	Density
CNT	Carbon nanotubes
Re	Reynold number
Pr	Prandtl number
Bi	Biot number
Rd	Thermal radiation parameter
Ω	Rotation parameter
SWCNTs	Single wall carbon nanotubes
MWCNTs	Multi wall carbon nanotubes

References

1. Choi, S.U.; Eastman, J.A. *Enhancing Thermal Conductivity of Fluids with Nanoparticles*; Argonne National Lab.: Lemont, IL, USA, 1995.
2. Nadeem, S.; Fuzhang, W.; Alharbi, F.M.; Sajid, F.; Abbas, N.; El-Shafay, A.; Al-Mubaddel, F.S. Numerical computations for Buongiorno nano fluid model on the boundary layer flow of viscoelastic fluid towards a nonlinear stretching sheet. *Alex. Eng. J.* **2021**, *61*, 1769–1778. [CrossRef]
3. Li, J.; Zhang, X.; Xu, B.; Yuan, M. Nanofluid research and applications: A review. *Int. Commun. Heat Mass Transf.* **2021**, *127*, 105543. [CrossRef]
4. Sreedevi, P.; Reddy, P.S. Effect of magnetic field and thermal radiation on natural convection in a square cavity filled with TiO_2 nanoparticles using Tiwari-Das nanofluid model. *Alex. Eng. J.* **2022**, *61*, 1529–1541. [CrossRef]
5. Ramzan, M.; Shahmir, N.; Alotaibi, H.; Ghazwani, H.A.; Muhammad, T. Thermal performance comparative analysis of nanofluid flows at an oblique stagnation point considering Xue model: A solar application. *J. Comput. Des. Eng.* **2022**, *9*, 201–215. [CrossRef]
6. Usman, M.; Hamid, M.; Zubair, T.; Haq, R.U.; Wang, W. Cu-Al_2O_3/Water hybrid nanofluid through a permeable surface in the presence of nonlinear radiation and variable thermal conductivity via LSM. *Int. J. Heat Mass Transf.* **2018**, *126*, 1347–1356. [CrossRef]
7. Hamid, M.; Usman, M.; Zubair, T.; Haq, R.U.; Wang, W. Shape effects of MoS2 nanoparticles on rotating flow of nanofluid along a stretching surface with variable thermal conductivity: A Galerkin approach. *Int. J. Heat Mass Transf.* **2018**, *124*, 706–714. [CrossRef]
8. Mohyud-Din, S.T.; Hamid, M.; Usman, M.; Kanwal, A.; Zubair, T.; Wang, W.; Nazir, A. Rotating flow of nanofluid due to exponentially stretching surface: An optimal study. *J. Algorithms Comput. Technol.* **2019**, *13*, 1748302619881365. [CrossRef]
9. Usman, M.; Haq, R.U.; Hamid, M.; Wang, W. Least square study of heat transfer of water based Cu and Ag nanoparticles along a converging/diverging channel. *J. Mol. Liq.* **2018**, *249*, 856–867. [CrossRef]
10. Wang, G.J.; Hadjiconstantinou, N.G. Why are fluid densities so low in carbon nanotubes? *Phys. Fluids* **2015**, *27*, 052006. [CrossRef]
11. Hayat, T.; Khan, S.A.; Alsaedi, A.; Zai, Q.Z. Computational analysis of heat transfer in mixed convective flow of *CNTs* with entropy optimization by a curved stretching sheet. *Int. Commun. Heat Mass Transf.* **2020**, *118*, 104881. [CrossRef]
12. Haq, R.U.; Nadeem, S.; Khan, Z.H.; Noor, N.F.M. Convective heat transfer in MHD slip flow over a stretching surface in the presence of carbon nanotubes. *Phys. B Condens. Matter* **2015**, *457*, 40–47. [CrossRef]
13. Mohyud-Din, S.T.; Usman, M.; Afaq, K.; Hamid, M.; Wang, W. Examination of carbon-water nanofluid flow with thermal radiation under the effect of Marangoni convection. *Eng. Comput.* **2017**, *34*, 2330–2343. [CrossRef]
14. Naqvi, S.M.R.S.; Muhammad, T.; Saleem, S.; Kim, H.M. Significance of non-uniform heat generation/absorption in hydromagnetic flow of nanofluid due to stretching/shrinking disk. *Phys. A Stat. Mech. Its Appl.* **2020**, *553*, 123970. [CrossRef]
15. Haq, R.; Khan, Z.; Khan, W. Thermophysical effects of carbon nanotubes on MHD flow over a stretching surface. *Phys. E Low-Dimens. Syst. Nanostruct.* **2014**, *63*, 215–222. [CrossRef]
16. Shah, Z.; Bonyah, E.; Islam, S.; Gul, T. Impact of thermal radiation on electrical MHD rotating flow of Carbon nanotubes over a stretching sheet. *AIP Adv.* **2019**, *9*, 015115. [CrossRef]

17. Khan, M.I.; Farooq, S.; Hayat, T.; Shah, F.; Alsaedi, A. Numerical simulation for entropy generation in peristaltic flow with single and multi-wall carbon nanotubes. *Int. J. Numer. Methods Heat Fluid Flow* **2019**, *29*, 4684–4705. [CrossRef]
18. Lu, D.; Ramzan, M.; Ahmad, S.; Chung, J.D.; Farooq, U. Upshot of binary chemical reaction and activation energy on carbon nanotubes with Cattaneo-Christov heat flux and buoyancy effects. *Phys. Fluids* **2017**, *29*, 123103. [CrossRef]
19. Saqib, M.; Khan, I.; Shafie, S. Application of Atangana–Baleanu fractional derivative to MHD channel flow of CMC-based-*CNTs* nanofluid through a porous medium. *Chaos Solitons Fractals* **2018**, *116*, 79–85. [CrossRef]
20. Saqib, M.; Khan, I.; Shafie, S. Natural convection channel flow of CMC-based *CNTs* nanofluid. *Eur. Phys. J. Plus* **2018**, *133*, 549. [CrossRef]
21. Asjad, M.I.; Aleem, M.; Ahmadian, A.; Salahshour, S.; Ferrara, M. New trends of fractional modeling and heat and mass transfer investigation of *(SWCNTs* and *MWCNTs)*-CMC based nanofluids flow over inclined plate with generalized boundary conditions. *Chin. J. Phys.* **2020**, *66*, 497–516. [CrossRef]
22. Soomro, F.A.; Haq, R.U.; Khan, Z.H.; Zhang, Q. Numerical study of entropy generation in MHD water-based carbon nanotubes along an inclined permeable surface. *Eur. Phys. J. Plus* **2017**, *132*, 412. [CrossRef]
23. Soomro, F.A.; Haq, R.U. *Mathematical Study of Convection Heat Transfer Utilizing Swcnt-Water Nanofluid Inside Partially Heated Hexagon Cavity*; ASTFE Digital Library, Begel House Inc.: Danbury, CT, USA, 2019.
24. Fan, S.; Wang, Y.; Cao, S.; Zhao, B.; Sun, T.; Liu, P. A deep residual neural network identification method for uneven dust accumulation on photovoltaic (PV) panels. *Energy* **2021**, *239*, 122302. [CrossRef]
25. Hamid, M.; Khan, Z.H.; Khan, W.A.; Haq, R.U. Natural convection of water-based carbon nanotubes in a partially heated rectangular fin-shaped cavity with an inner cylindrical obstacle. *Phys. Fluids* **2019**, *31*, 103607. [CrossRef]
26. Khan, Z.H.; Khan, W.A.; Haq, R.; Usman, M.; Hamid, M. Effects of volume fraction on water-based carbon nanotubes flow in a right-angle trapezoidal cavity: FEM based analysis. *Int. Commun. Heat Mass Transf.* **2020**, *116*, 104640. [CrossRef]
27. Khan, Z.H.; Khan, W.A.; Hamid, M.; Liu, H. Finite element analysis of hybrid nanofluid flow and heat transfer in a split lid-driven square cavity with Y-shaped obstacle. *Phys. Fluids* **2020**, *32*, 093609. [CrossRef]
28. Nguyen-Thoi, T.; Sheikholeslami, M.; Hamid, M.; Haq, R.-U.; Shafee, A. CVFEM modeling for nanofluid behavior involving non-equilibrium model and Lorentz effect in appearance of radiation. *Phys. A Stat. Mech. Its Appl.* **2019**, *534*. [CrossRef]
29. Sheikholeslami, M.; Hamid, M.; Haq, R.U.; Shafee, A. Numerical simulation of wavy porous enclosure filled with hybrid nanofluid involving Lorentz effect. *Phys. Scr.* **2020**, *95*, 115701. [CrossRef]
30. Ellahi, R.; Zeeshan, A.; Waheed, A.; Shehzad, N.; Sait, S.M. Natural convection nanofluid flow with heat transfer analysis of carbon nanotubes–water nanofluid inside a vertical truncated wavy cone. *Math. Methods Appl. Sci.* **2021**. [CrossRef]
31. Khan, Z.H.; Khan, W.A.; Sheremet, M.A.; Hamid, M.; Du, M. Irreversibilities in natural convection inside a right-angled trapezoidal cavity with sinusoidal wall temperature. *Phys. Fluids* **2021**, *33*, 083612. [CrossRef]
32. Khan, Z.; Hamid, M.; Khan, W.; Sun, L.; Liu, H. Thermal non-equilibrium natural convection in a trapezoidal porous cavity with heated cylindrical obstacles. *Int. Commun. Heat Mass Transf.* **2021**, *126*, 105460. [CrossRef]
33. Dadheech, P.K.; Agrawal, P.; Mebarek-Oudina, F.; Abu-Hamdeh, N.H.; Sharma, A. Comparative heat transfer analysis of MoS2/C2H6O2 and SiO2-MoS2/C2H6O2 nanofluids with natural convection and inclined magnetic field. *J. Nanofluids* **2020**, *9*, 161–167. [CrossRef]
34. Dhif, K.; Mebarek-Oudina, F.; Chouf, S.; Vaidya, H.; Chamkha, A.J. Thermal Analysis of the Solar Collector Cum Storage System Using a Hybrid-Nanofluids. *J. Nanofluids* **2021**, *10*, 616–626. [CrossRef]
35. Chabani, I.; Mebarek-Oudina, F.; Ismail, A.A.I. MHD Flow of a Hybrid Nano-Fluid in a Triangular Enclosure with Zigzags and an Elliptic Obstacle. *Micromachines* **2022**, *13*, 224. [CrossRef] [PubMed]
36. Pushpa, B.V.; Sankar, M.; Mebarek-Oudina, F. Buoyant Convective Flow and Heat Dissipation of Cu–H_2O Nanoliquids in an Annulus Through a Thin Baffle. *J. Nanofluids* **2021**, *10*, 292–304. [CrossRef]
37. Marzougui, S.; Mebarek-Oudina, F.; Magherbi, M.; Mchirgui, A. Entropy generation and heat transport of Cu–water nanoliquid in porous lid-driven cavity through magnetic field. *Int. J. Numer. Methods Heat Fluid Flow* **2021**. [CrossRef]
38. Fan, S.; Wang, Y.; Cao, S.; Sun, T.; Liu, P. A novel method for analyzing the effect of dust accumulation on energy efficiency loss in photovoltaic (PV) system. *Energy* **2021**, *234*, 121112. [CrossRef]
39. Stewartson, K. On the flow between two rotating coaxial disks. In *Mathematical Proceedings of the Cambridge Philosophical Society*; Cambridge University Press: Cambridge, UK, 1953; pp. 333–341.
40. Imtiaz, M.; Hayat, T.; Alsaedi, A.; Ahmad, B. Convective flow of carbon nanotubes between rotating stretchable disks with thermal radiation effects. *Int. J. Heat Mass Transf.* **2016**, *101*, 948–957. [CrossRef]
41. Usman, M.; Din, S.T.M.; Zubair, T.; Hamid, M.; Wang, W. Fluid flow and heat transfer investigation of blood with nanoparticles through porous vessels in the presence of magnetic field. *J. Algorithms Comput. Technol.* **2018**, *13*. [CrossRef]
42. Usman, M.; Hamid, M.; Din, S.T.M.; Waheed, A.; Wang, W. Exploration of uniform heat flux on the flow and heat transportation of ferrofluids along a smooth plate: Comparative investigation. *Int. J. Biomath.* **2018**, *11*. [CrossRef]
43. Usman, M.; Hamid, M.; Rashidi, M.M. Gegenbauer wavelets collocation-based scheme to explore the solution of free bio-convection of nanofluid in 3D nearby stagnation point. *Neural Comput. Appl.* **2018**, *31*, 8003–8019. [CrossRef]

44. Cai, T.; Dong, M.; Liu, H.; Nojavan, S. Integration of hydrogen storage system and wind generation in power systems under demand response program: A novel p-robust stochastic programming. *Int. J. Hydrog. Energy* **2021**, *47*, 443–458. [CrossRef]
45. Hamid, M.; Usman, M.; Haq, R.U.; Tian, Z. A spectral approach to analyze the nonlinear oscillatory fractional-order differ-ential equations. *Chaos Solitons Fractals* **2021**, *146*, 110921. [CrossRef]